*Blind Deconvolution for Single Noisy and Blurry Image Using Alternating Maximum a Posteriori Estimation with Low Rank Prior**

Shijie Sun[*†‡§], Huaici Zhao[*‡§], Jinfeng Lv[*†‡§], Mingguo Hao[*‡§] and Bo Li[*†‡§¶]

[*]Shenyang Institute of Automation, Chinese Academy of Sciences, Shenyang, China
[†]University of Chinese Academy of Science, Beijing, China
[‡]Key Laboratory of Optical-Electronics Information Processing, Chinese Academy of Sciences, Shenyang, China
[§]Key Laboratory of Image Understanding and Computer Vision, Shenyang, China
[¶]College of Information, Shenyang Institute of Engineering, Shenyang, China
Email: {sunshijie, hczhao, lvjinfeng, hmg, leebo}@sia.cn

***Abstract*—The purpose of single image blind deconvolution is to estimate the unknown blur kernel from a single observed blurred image and recover the original sharp image. Such task is severely ill-posed and even more challenging especially in the condition that the noise in the input image cannot be negligible. In this paper, the main problem we focus on is how to effectively apply low rank prior to blind deconvolution. A single noisy and blurry image blind deconvolution algorithm is proposed, using alternating maximum a posteriori (MAP) estimation combined with low rank prior. When estimating the intermediate latent image, low rank prior is used as the constraint that is used for noise suppression of the restored image. The denoised intermediate latent image in turn leads to higher quality blur kernel estimation. These two operations are iterated in this manner to arrive at reliable blur kernel estimation. Extensive experiments show the superiority of the proposed method over state-of-the-art techniques, both qualitatively and quantitatively.**

Keywords—MAP; blind deconvolution; low rank prior; noise

I. INTRODUCTION

Image deconvolution (also known as image deblurring), which has attracted considerable attention owing to its involvement of many challenges in problem formulation, regularization and optimization, is one of the most fundamental problems in computer vision and image processing community[1-19]. Image blur often stems from the relative motion between a camera and the scene during the exposure time. It can lead to significant image degradation, especially in low light conditions where longer exposure time and higher ISO setting are required. Although the blur effect can be overcome by selecting a faster shutter speed, it inevitably leads to a large amount of noise.

Most existing methods consider the image blur as a convolution process with a uniform blur kernel on a latent input image, and have achieved a fair level of success on photos with little image noise. However, larger degrees of noise can significantly impair these algorithms. When low noise assumption is not true, image noise may manifest itself as noise in the estimated blur kernel, which can result in the inaccuracy kernel estimation. Furthermore, image noise can also be amplified by deconvolution, which results in severe artifacts in the restored latent image. Thus, blur kernel estimation is quite difficult in the case that the noise is large enough for the blurred image. Up to now, blind deconvolution for noisy and blurry images has not yet received enough attention. Although several methods [13] has been proposed lately for dealing with this problem, it's still a challenge to reliably estimate the accurate blur kernel from a noisy blurred image and recover the original sharp image.

In this paper, a single noisy blurred image blind deconvolution algorithm is proposed, taking advantage of alternating maximum a posteriori (MAP) estimation combined with low rank prior. Low rank prior has been successfully employed to deal with many image processing problems (i.e., image denoising). In our approach, low rank prior is effectively incorporated into an alternating MAP estimation framework of blind deconvolution. Thus, the problem of blur kernel estimation can be addressed by iteratively solving intermediate latent image restoration and kernel estimation, and then the final latent image is recovered by using a non-blind deconvolution method. Experimental results manifest that the proposed method achieves state-of-the-art results.

II. RELATED WORK

A. Spatially Invariant Blur

The problem of removing spatially invariant blur has been extensively studied and rather significant progress has been made. For single image deblurring, recent works focus on estimating a complex motion blur kernel from a single image. The success of these methods is partly due to the employment of sparse priors and the multi-scale framework. Fergus *et al.* [1] used a zero-mean Mixture of Gaussian to fit the heavy-tailed distribution of natural image gradients. A variational Bayesian framework was employed to deblur an image. Shan *et al.* [2] exploited a unified probabilistic model for both the latent image and blur kernel. Deblurring is achieved via an alternating minimization scheme. Cai *et al.* [3] considered that the latent images and kernels could be sparsely represented by an over-complete dictionary, and then adopted a framelet and curvelet system to obtain the sparse representation for kernels and images. Levin *et al.* [4] demonstrated the limitation of the common MAP methods involving estimating both the image and kernel, and proposed an efficient marginal likelihood approximation. [5] Krishnan *et al.* [6] applied a new normalized sparsi-

*This work is in part supported by the General Scientific Research Project of Education Department of Liaoning of China under Grant No. L2015368

978-1-5090-4099-5/16/$31.00 ©2016 IEEE

ty prior to blind kernel estimation. Sun *et al*. [7] introduced a new patch-based prior to estimating blur kernel. Mai *et al*. [8] proposed a data-driven approach to fuse multiple blur kernels estimated from different existing deblurring methods into a more accurate one. A Gaussian Conditional Random Fields-based fusion method was developed to obtain the final blur kernel. Remarkably, blur kernels estimated from the aforementioned works usually contain some noise.

Another group of methods employed an explicit edge prediction step for blur kernel estimation. Especially, Joshi *et al*. [9] predicted sharp edges by first locating step edges and then propagating the local intensity extrema towards the edge. This method was adopted to handle complex blur kernels using a multi-scale scheme. Cho and Lee [10] applied bilateral filtering together with shock filtering to predict sharp edges and then selected the salient edges for kernel estimation. Xu and Jia [11] analyzed the effect of the scale of blurred edges on kernel estimation, and developed an edge selection method for robust blur kernel estimation. The kernel refinement was implemented using iterative support detection (ISD) technique. Pan *et al*. [12] further proposed an new mask computation algorithm, adaptively selecting useful edges for kernel estimation. Zhong et al. [13] showed that directly applying image denoising methods partially damaged the blur information, leading to biased kernel estimation, and then used directional filters together with Radon transform to estimate the blur kernel from a noisy blurred image. Zhou *et al*. [14] imposed a geometric parsing prior on general MAP-estimation framework for blind image deblurring. Although the performance of these methods is greatly improved, the estimated kernels still include some noise occasionally, the sparsity of which also cannot be guaranteed. For multiple images deblurring, some algorithms have also been developed, making the effort to combine complementary information from multiple images for generating higher quality image estimation. Interested readers can refer to [15][16] for more details.

B. *Spatially Variant Blur*

Removing spatially variant blur is a challenging task in which regions are degraded differently, hence entailing non-uniform models over the entire image. This problem has recently attracted more attention for its wide range of practical applications. One approach to deal with spatially variant blur is to segment the blurry image into multiple regions where each one is modelled by a uniform blur kernel. This method is sensible and well-known uniform image deblurring algorithms can be used when the segments are determined. However, these segmented regions often need to be small enough to meet the assumption of using uniform blur kernels. Another approach is to model or capture the camera motion during the blur process and obtain spatially variant blur kernels at different sites. More details can be found in [17][18][19].

III. BLIND DECONVOLUTION BASED ON MAP ESTIMATION

For spatially invariant blur, the formation process of image blur is often represented as

$$g = u * h + n, \tag{1}$$

where u is the sharp latent image, h is the blur kernel (a.k.a. point spread function), n is the image noise (this paper assumes i.i.d. additive white Gaussian noise), "$*$" denotes convolution operator and g is the observed blur image. In blind image deconvolution, estimating both h and u from g is a well-known ill-posed inverse problem, and the additional noise n also makes this problem even more challenging.

From probabilistic point of view, simultaneous recovery of u and h in Eq. (1) amounts to solving standard MAP estimation, seeking a pair $(\hat{u},\hat{h})$ maximizing

$$\begin{aligned} P(u,h|g) &\propto P(g|u,h)P(u,h) \\ &= P(g|u,h)P(u)P(h), \end{aligned} \tag{2}$$

where the likelihood term $P(g|u,h)$ is the noise distribution $\log P(g|u,h) = -\frac{\gamma}{2}\|u*h-g\|^2$ (in this case assumed Gaussian) and also known as the data fitting term, $P(u)$ and $P(h)$ are the prior distributions on latent image and blur kernel, respectively. The prior $P(u)$ favors natural images, mainly stemming from the observation that their gradient distribution is sparse. A popular measure is

$$\begin{aligned} J_u(u) &= \Phi(D_x u, D_y u) = -\log P(u) \\ &= \sum_i \left([D_x u]_i^2 + [D_y u]_i^2 \right)^{\frac{\alpha}{2}} + C, \ 0 \le \alpha \le 1 \end{aligned} \tag{3}$$

where D_x and D_y denote the horizontal and vertical derivative operators, respectively. $[u]_i$ denotes the i-th component of the vector $[u]$, which is lexicographically ordered vector representation of the latent image u. C is a constant normalization term. For the blur kernel, the prior $P(h)$ is usually expressed by adopting distribution on the positive kernel values to force sparsity and zero on the negative values, which can be formulated as

$$J_h(h) = \Psi(h) = -\log P(h) = \frac{1}{2}\sum_i \left(|[h]_i| + |[h]_i| \right), \tag{4}$$

in which $[h]_i$ denotes i-th component of the vector $[h]$.

Hence maximizing the posteriori $P(g|u,h)$ in Eq. (2) is equivalent to seeking $(\hat{u},\hat{h})$ minimizing its negative logarithm, i.e.,

$$\begin{aligned} (\hat{u},\hat{h}) &= \arg\min_{u,h} \{ -\log(P(u,h|g)) \} \\ &= \arg\min_{u,h} \frac{\gamma}{2}\|u*h-g\|_2^2 + \lambda J_u(u) + \eta J_h(h), \end{aligned} \tag{5}$$

where λ and η are the relative regularization weight for the latent image u and blur kernel h respectively.

IV. OUR APPROACH

In blind deconvolution for single noisy and blurry image, the purpose is to recover both the latent image u and blur kernel h given the noisy and blurry observation g. To that end, here an auxiliary variable L is introduced and Eq. (5) can be rewritten as follows:

$$(\hat{u},\hat{h},L)=\arg\min_{u,h,L}\frac{\gamma}{2}\|h*u-g\|_2^2+\lambda J_u(u)+\beta J_h(h)+\tau J_{LR}(u,L)\,, \tag{6}$$

where L is a denoised blur image in vector form, τ is the regularization parameter, and $J_{LR}(u,L)$ is the low rank prior term and defined as

$$J_{LR}(u,L)=\sum_i^N\|R_iu-L_i\|_F^2+\eta\|L_i\|_*\,, \tag{7}$$

where R_i denotes a matrix which is used to extract an image patch from the i-th position, $R_iu=[u_{i1},u_{i2},\cdots u_{iN}]\in\mathbb{R}^{n\times N}$ is the i-th set of similar image patches (with noise) extracted from the image u via k-Nearest-Neighbor method, L_i is the restored image patches without noise in vector form, $\|\cdot\|_F^2$ is the Frobenious norm, $\|\cdot\|_*$ and η denote the nuclear norm (i.e., sum of the singular values) and the regularization parameter, respectively. The introduction of L allows us to separate the processes of image denoising and blind deconvolution, effectively improving the intermediate latent image restoration playing a critical role in kernel estimation process. The low rank prior term will be further explained in the following section.

In this work, an alternating coarse-to-fine optimization framework is developed to solve Eq. (6) for enhancing the accuracy of blur kernel estimation. Our approach first starts with a denoised blurry image L computed by using an existing denoising algorithm. Then, L is refined by using the nonlocal self-similarity constraint on u, which also can avoid over-sharpening or over-smoothing in the denoised image. With the updated L, u is refined again. The two alternating procedures are iterated to refine u and L to estimate a more accurate h. Finally, h is estimated from the refined u. At each image level, the above iterations of alternating optimization is run to refine L, u and h. To obtain a better latent image with finer textures, the final latent image is recovered via non-blind deconvolution method. Fig. 1 summarizes the main steps for solving Eq. (6).

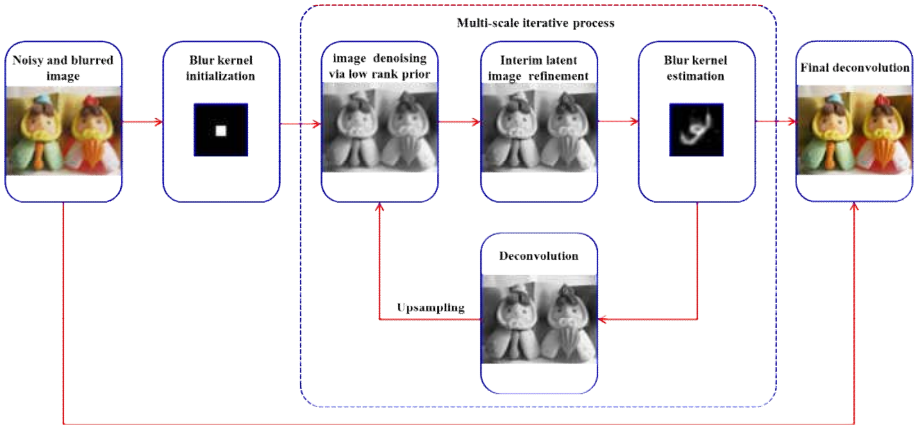

Fig. 1. Main steps of the proposed algorithm.

A. Optimization Algorithm

Solving Eq. (6) is difficult because it contains even more unknowns than Eq. (5). In order to numerically find the solution L, u and h, the alternating minimization scheme is employed, which separately optimizes Eq. (6) with respect to L, u or h while keeping the other constant.

Next, the optimization process is described in detail.

1) *Optimizing over the intermediate latent image* u **and** L

When the blur kernel h is kept fixed, optimization of Eq. (6) over u *and* L amounts to the following problem

$$(\hat{u},\hat{L})=\arg\min_{u,L}\frac{\gamma}{2}\|h*u-g\|_2^2+\lambda\Phi(D_xu,D_yu)+\tau J_{LR}(u,L)\,. \tag{8}$$

Minimizing Eq. (8) involves simultaneously solving two variables: u and L, which is computationally challenging. To efficiently obtain a set of solution of Eq. (8), here the alternating minimization scheme is adopted to deal with this problem.

a) ***Optimizing over*** u. With L fixed, the problem for estimating the intermediate latent image u is equivalent to solving

$$\hat{u}=\arg\min_u\frac{\gamma}{2}\|h*u-g\|_2^2+\tau\sum_i^N\|R_iu-L_i\|_F^2+\lambda\Phi(D_xu,D_yu)\,. \tag{9}$$

For Eq. (9), it contains non-linear penalties for the data and regularization terms. The augmented Lagrangian method [20] (ALM) can be used to effectively solve it by introducing new variables $v_x=D_xu$, $v_y=D_yu$ and their corresponding quadratic penalty term, which results in the following object function

$$(\hat{u},\hat{v}_x,\hat{v}_y)=\arg\min_{u,v_x,v_y}\frac{\gamma}{2}\|h*u-g\|_2^2+\tau\sum_i^N\|R_iu-L_i\|_F^2+\lambda\Phi(v_x,v_y)+\frac{\mu}{2}\left(\|D_xu-v_x-a_x\|_2^2+\|D_yu-v_y-a_y\|_2^2\right), \tag{10}$$

where the new variables a_x and a_y are proportional to the estimates of the Lagrange multipliers of the corresponding constraints, and μ is the penalty weight. After such reformulation, the data term $\|h*u-g\|_2^2$ and the regularization term $\Phi(v_x,v_y)$ can be optimized separately as they depend on different variables. Moreover, by adding penalty terms, ALM allows us to treat the constrained variables D_xu and v_x (similarly D_yu

and v_y) as if they were unrelated. Thus by keeping the penalty weight μ sufficiently large, the solution of Eq. (10) approaches that of Eq. (9).

With the adjusted formulation, Eq. (10) can now be computed by an efficient Alternating Minimization scheme. The operations are iterated among solving u, v_x and v_y independently by fixing other variables. v_x, v_y, a_x and a_y are initialized to zeros.

At each iteration, u is first computed given the initial or estimated v_x, v_y, a_x and a_y by minimizing the following object function

$$\hat{u} = \arg\min_u \frac{\gamma}{2}\|h*u-g\|_2^2 + \tau\sum_i^N \|R_i u - L_i\|_F^2 + \frac{\mu}{2}\left(\|D_x u - v_x - a_x\|_2^2 + \|D_y u - v_y - a_y\|_2^2\right). \quad (11)$$

Eq. (11) is equivalent to Eq. (10) after removing constant. As a quadratic function, Eq. (11) bears a closed form solution that can be obtained by using Fast Fourier Transform (FFT). The optimal u is written as

$$u = \mathcal{F}^{-1}\left(\frac{\overline{\mathcal{F}(h)}\mathcal{F}(g) + \frac{\mu}{\gamma}\left(\overline{\mathcal{F}(\partial_x)}\mathcal{F}(v_x+a_x) + \overline{\mathcal{F}(\partial_y)}\mathcal{F}(v_y+a_y)\right) + \frac{\tau}{\gamma}\mathcal{F}(\sum_i R_i^T L_i)}{\overline{\mathcal{F}(h)}\mathcal{F}(h) + \frac{\mu}{\gamma}\left(\overline{\mathcal{F}(\partial_x)}\mathcal{F}(\partial_x) + \overline{\mathcal{F}(\partial_y)}\mathcal{F}(\partial_y)\right) + \frac{\tau}{\gamma}\mathcal{F}(\sum_i R_i^T R_i)}\right) \quad (12)$$

where $\mathcal{F}(\cdot)$ and $\mathcal{F}^{-1}(\cdot)$ denote the FFT and inverse FFT, respectively. $\overline{\mathcal{F}(\cdot)}$ is the complex conjugate operator. Derivative operators D_x and D_y are implemented by using the simple filters $\partial_x = [1, -1]$ and $\partial_y = [1, -1]^T$.

In solving for v_x and v_y given the u estimation, the terms not depending on v_x and v_y in Eq. (10) can be disregarded. The optimal v_x and v_y can be obtained by minimizing the following object function

$$\begin{aligned}(\hat{v}_x, \hat{v}_y) &= \arg\min_{v_x, v_y} \frac{\lambda}{\mu}\Phi(v_x, v_y) + \frac{1}{2}\|D_x u - v_x - a_x\|_2^2 \\ &\quad + \frac{1}{2}\|D_y u - v_y - a_y\|_2^2 \\ &= \arg\min_{v_x, v_y} \frac{\lambda}{\mu}\sum_i \left([v_x]_i^2 + [v_y]_i^2\right)^{\frac{\alpha}{2}} + \frac{1}{2}\sum_i \left([v_x]_i - \left([D_x u]_i - [a_x]_i\right)\right)^2 \\ &\quad + \frac{1}{2}\sum_i \left([v_y]_i - \left([D_y u]_i - [a_y]_i\right)\right)^2, \end{aligned} \quad (13)$$

where each term perform a corresponding summation over all image pixels. Therefore, derivatives and minimization can be implemented pixel by pixel independently. Let i be a pixel index, $t = \left([v_x]_i, [v_y]_i\right)$ and $r = \left([D_x u]_i - [a_x]_i, [D_y u]_i - [a_y]_i\right)$, then Eq. (13) for each pixel can be reformulated as

$$\hat{t} = \arg\min_t \frac{\lambda}{\mu}\|t\|^\alpha + \frac{1}{2}\|t - r\|^2, \quad (14)$$

where $\|\cdot\|$ denotes the conventional vector 2-norm. For the general case $0 < \alpha < 1$, Eq. (14) bears no closed form solution. However, because α is known beforehand and Eq. (14) is basically 1D minimization problem, the approximate solution of Eq. (14) can be precomputed numerically off-line and tabulated to form a lookup table (LUT). Thus the LUT can be used independently for each i-th component of $\left(v_x, v_y\right)$.

For the variables a_x and a_y, they can be updated according to the strategy of gradient descent.

b) ***Optimizing over*** L. With u fixed, the problem for updating L is equivalent to solving function

$$\hat{L} = \arg\min_L \sum_i \|R_i u - L_i\|_F^2 + \eta\|L_i\|_*. \quad (15)$$

It is a standard low-rank matrix approximation problem [21].

For each L_i, the closed form solution can be obtained by

$$\begin{cases}(U_i, \Sigma_i, V_i) = svd(R_i u) \\ L_i = U_i \mathcal{D}_{\eta/2}(\Sigma_i) V^*\end{cases} \quad (16)$$

where (U_i, Σ_i, V_i) is the singular value decomposition (SVD), $\mathcal{D}_{\eta/2}$ denotes the soft-thresholding operator with threshold $\eta/2$ and defined as

$$\mathcal{D}_{\eta/2}(\Sigma) = \text{diag}\left(\{\sigma_i - \frac{\eta}{2}\}_+\right), \quad (17)$$

where $\Sigma = \text{diag}(\{\sigma_i\})$ and σ_i is the singular value, $x_+ = \max(0, x)$.

Based on the above analysis, our alternating minimization algorithm for the intermediate latent image restoration is summarized in Alg. 1.

Algorithm 1 Intermediate latent image restoration via low rank regularization

Input: Blur image g and blur kernel h

initialization:

(a) Set $v_x^0 = 0$, $v_y^0 = 0$, $a_x^0 = 0$, $a_y^0 = 0$ and $j = 0$.

(b) Set parameters λ, γ, τ, μ and η.

repeat

(a) Solve for L^{j+1} by minimizing Eq. (15).

(b) Solve for u^{j+1} by minimizing Eq. (11).

(c) Update the vector $([v_x^{j+1}]_i, [v_y^{j+1}]_i)$ $([v_x^{j+1}]_i, [v_y^{j+1}]_i) = \text{LUT}([D_x u^{j+1} - a_x^j]_i, [D_y u^{j+1} - a_y^j]_i), \forall i$.

(d) Update the variable $a_x^{j+1} = a_x^j - D_x u^{j+1} + v_x^{j+1}$.

(e) Update the variable $a_y^{j+1} = a_y^j - D_y u^{j+1} + v_y^{j+1}$.

(f) $j \leftarrow j + 1$.

until $\|u^{j+1} - u^j\|_2 / \|u^j\|_2 \le \varepsilon$ ($\varepsilon = 1e^{-3}$ empirically) or the maximum iteration limit is reached (here set j to 10).

Output: Latent image u^j.

B. Optimizing over the Blur Kernel h

When the intermediate latent image u is kept fixed, optimization of Eq. (6) over h amounts to the following problem

$$\hat{h} = \arg\min_{h} \frac{\gamma}{2}\|h * u - g\|_2^2 + \beta\Psi(h). \tag{18}$$

To separate the minimization of data term and regularization term, minimizing with respect to h can be done in a fashion similar to the optimization over u. By introducing the substitution $v_h = h$, Eq. (18) is equivalent to solving

$$(\hat{h}, \hat{v}_h) = \arg\min_{h, v_h} \frac{\gamma}{2}\|h * u - g\|_2^2 + \beta\Psi(v_h) + \frac{\delta}{2}\|h - v_h - a_h\|_2^2, \tag{19}$$

Where a_h is proportional to the estimate of the Lagrange multiplier of the prescribed constraint and δ is the penalty weight. Eq. (19) can be computed given the initial or estimated v_h and a_h by minimizing the following object function

$$\hat{h} = \arg\min_{h, v_h} \frac{\gamma}{2}\|h * u - g\|_2^2 + \frac{\delta}{2}\|h - v_h - a_h\|_2^2. \tag{20}$$

As a quadratic function, Eq. (20) also bears a closed form solution in minimization and can be solved by using FFT. The optimal h is written as

$$h = \mathcal{F}^{-1}\left(\frac{\overline{\mathcal{F}(u)}\mathcal{F}(g) + \frac{\delta}{\gamma}\mathcal{F}(v_h + a_h)}{\overline{\mathcal{F}(u)}\mathcal{F}(u) + \frac{\delta}{\gamma}\mathcal{F}(I)}\right) \tag{21}$$

where I denotes identity matrix.

In solving for v_h given the h estimation, the terms not depending on v_h in Eq. (19) can be removed. The optimal v_h can be obtained by minimizing the following object function

$$\hat{v}_h = \arg\min_{v_h} \beta\Psi(v_h) + \frac{\delta}{2}\|h - v_h - a_h\|_2^2 = \arg\min_{v_h} \frac{\beta}{\delta}\sum_i \Psi([v_h]_i) + \frac{1}{2}\sum_i \left([v_h]_i - ([h]_i - [a_h]_i)\right)^2. \tag{22}$$

Computing v_h also can be done component-wise and even simpler. Let i be a pixel index, $t = [v_h]_i$ and $r = [h - a_h]_i$, then Eq. (22) for each pixel can be rewritten as $\arg\min_t \beta/\delta\,\Psi(t) + 1/2\,(r-t)^2$, which is the scalar version of Eq. (14) for $\alpha = 1$ with the additional constraint that only positive values of t are allowed. Thus the solution of Eq. (22) can be derived according to the component-wise shrinkage formula

$$[v_h]_i = \max([h - a_h]_i - \frac{\delta}{\beta}, 0) \tag{23}$$

Computing the variable a_h also can be implemented according to the strategy of gradient descent.

Based on the above analysis, our minimization algorithm for the blur kernel is summarized in Alg. 2.

Algorithm 2 Blur kernel estimation algorithm

Input: Latent image u and blur image g

initialization:

(a) Set $v_h^0 = 0$, $a_h^0 = 0$, and $j = 0$.

(b) Set parameters γ, β, and δ.

repeat

(a) Solve for h^{j+1} by minimizing Eq. (20).

(b) Update the variable $[v_x^{j+1}]_i$ $(\forall i)$ according to Eq. (23).

(c) Update the variable $a_h^{j+1} = a_h^j - h^{j+1} + v_h^{j+1}$.

(d) $j \leftarrow j + 1$.

until $\|h^{j+1} - h^j\|_2 / \|h^j\|_2 \le \varepsilon$ ($\varepsilon = 1e^{-3}$ empirically) or the maximum iteration limit is reached (here set j to 10).

Output: Blur kernel h^j.

In order to increase the accuracy of kernel estimation, we adopt the iterative coarse-to-fine optimization framework that is commonly used in recent methods. Alg. 3 presents the main steps in one image level.

Algorithm 3 The complete blur kernel estimation algorithm in one image level

Input: Blur image g.

Initialization u and h from the previous coarser-scale level.

for $j = 1 \to 10$ (the maximum iteration limit)

(a) Estimate h by Alg. 2.

(b) Estimate u by Alg. 1.

(c) Update $\gamma \leftarrow 3\gamma/2$

end for

Output: Blur kernel h.

C. Final Latent Image Restoration

In the final deconvolution step, we employ the estimated blur kernel h to generate a good latent image u from the noisy and blurry input g. However, this is not a trivial task when the input g contains severe noise. Most of the previous non-blind deconvolution algorithms cannot work well when image noise is non-negligible. In order to obtain a better latent image with finer textures, we adopt the non-blind deconvolution method in [13] to estimate the final latent image, which is defined as

$$\hat{u} = \arg\min_{u} \|g * h - u\|_2^2 + w\|u - NLM(u)\|_2^2 \tag{24}$$

where $NLM(\cdot)$ is the non-local means denoising operation, and w is a balancing weight and empirically set to 0.5.

V. Experimental Results

In this section, we first verified our algorithm on the image test set introduced in [5], and then conducted experiments on the real world images provided in [9]. On this basis, we compared our results with those of several state-of-the-art single image deblurring methods for spatially invariant blur.

For all the experiments, some implementation details are as follows. In the kernel estimation, all color images are convert-

ed to grayscale ones. For our experiments, we use $\gamma = 1$ to estimate blur kernels and then multiply the γ by 1.5 after each pass of the u -estimation and h -estimation pair. We use $\tau = 10^{-2}$ and $\mu = 1$ in Eq. (11), $\lambda = 1$ and $\alpha = 0.3$ in Eq. (14), $\beta = 1$ and $\delta = 10^4$ in Eq. (19). The parameter η in Eq. (15) is chosen according to [21], and w in Eq. (24) is set to 0.5. In the final latent image estimation, each color channel is processed separately. We implemented our method in Matlab on a PC running MS Windows 8 64bit version with Intel Core i5 CPU 2.20GHz and 8GB RAM.

We make use of three measurements for quantitative analysis: kernel similarity introduced in [22], mean PSNR and mean SSIM employed in [23].

A. *Quantitative evaluation of the synthetic test dataset*

The synthetic dataset in [4] contains 32 test images produced from 4 sharp grayscale images of size 255×255 and 8 real-world blur kernels, as shown in Fig. 2 and available online.[1] On the basis of this dataset, we respectively added 2% and 5% additive Gaussian noise by using Photoshop to simulate the effects of camera noise, which produced two test sets with different noise levels. Furthermore, we employed the kernel similarity between the estimated kernels and the ground truth, which is first used in [22], to measure the quality of the estimated results. We compare our method with those of Krishnan *et al.* [6], Xu and Jia [11], Pan *et al.* [12] and Zhong *et al.* [13]. Fig. 3 shows the kernel similarity performance, which suggests that overall our method outperforms other competing methods on the two test sets. We also employ mean Peak Signal-to-Noise Ratio (PSNR) and mean Structural SIMilarity (SSIM) to quantitatively evaluate the estimation accuracy for the restored image. The results are shown in Fig. 4. Our method provides both higher mean PSNR value and mean SSIM value.

Fig. 2. The dataset of [4]. First row is sharp images, second row is real-world kernels.

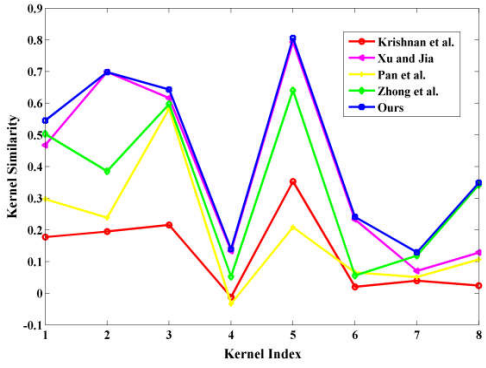

(a)

[1] www.wisdom.weizmann.ac.il/~levina/papers/LevinEtalCVPR09Data.zip

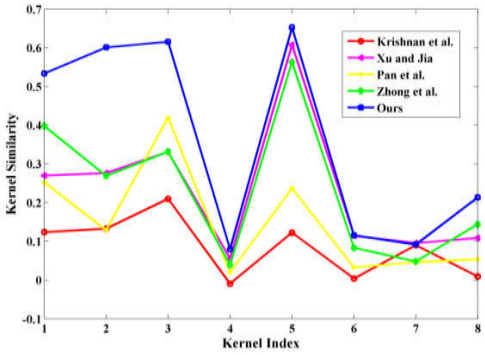

(b)

Fig. 3. Performance comparison of kernel similarity with state-of-the-art methods on the synthetic dataset. (a) Test with 2% additive Gaussian noise. (b) Test with 5% additive Gaussian noise. The x-axis denotes the blur kernel index. Overall our method performs the best.

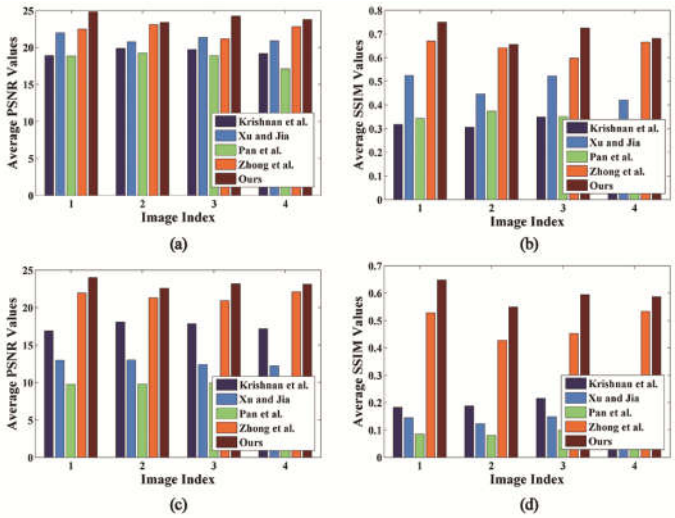

Fig. 4. Quantitative comparison on the synthetic dataset. (a) and (b) denote the values of PSNR and SSIM with 2% additive Gaussian noise. (c) and (d) denote the values of PSNR and SSIM with 5% additive Gaussian noise. The x-axis denotes the image index. Overall our method performs the best.

B. *Evaluation on real noisy and blurred images*

All test images in [4] are 255×255 in size and limited in terms of diversity. In order to further verify the effectiveness of our approach, we conducted experiments on real noisy and blurred images of low-light scenes, which are provided in [24]. Then we compare our results with those of other state-of-the-art methods, including Krishnan *et al.* [6], Xu and Jia [11], Pan *et al.* [12] and Zhong *et al.* [13]. The results are shown in Fig. 5 and Fig. 6. Obviously, our algorithm outperforms these methods run with optimum parameters for deblurring. Moreover, our recovered latent images contain fewer artifacts and include more high-frequency details.

VI. CONCLUSIONS

In this paper, we have proposed an effective method for blind deblurring of noisy and blurry images. The proposed method incorporates low rank prior into the MAP-based blind image deblurring framework. In the intermediate latent image

restoration, low rank prior can effectively suppress noise in the restored latent image, which in turn provides more reliable for the kernel estimation. The combination greatly improves the quality of kernel estimation. Both quantitative and qualitative evaluations on challenging examples demonstrate that the proposed method performs favorably against several state-of-the-art algorithms.

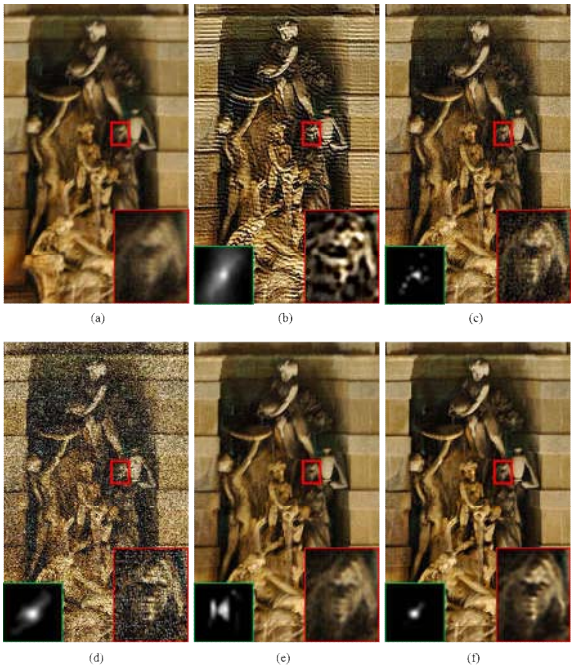

Fig. 5. A real world image with unknown camera shake. (a) Input noisy and blurry image. (b) Result from Krishnan *et al*. (c) Result from Pan *et al.* (d) Result from Xu and Jia. (e) Result from Zhong *et al*. (f) Our result. The estimated blur kernel and zoom-in regions are also shown. Our result contains more high-frequency details and fewer ringing artifacts.

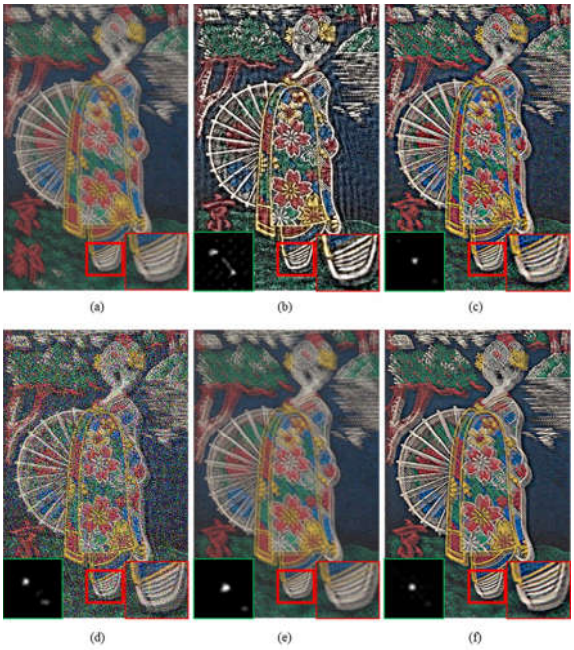

Fig. 6. Another real world image with unknown camera shake. (a) Input noisy and blurry image. (b) Result from Krishnan *et al*. (c) Result from Pan *et al.* (d) Result from Xu and Jia. (e) Result from Zhong *et al*. (f) Our result. Our method produces competitive results.

REFERENCES

[1] Fergus R et al., "Removing camera shake from a single photograph," ACM Trans. on Graph. vol. 25, no. 3, pp. 787-794, 2006.

[2] Shan Q, Jia J Y, and Agarwala A, "High-quality motion deblurring from a single image," ACM Trans. on Graphs. vol. 27, no. 3, pp. 787-794, 2006.

[3] Cai J F et al., "Blind motion deblurring from a single image using sparse approximation," in Proc. IEEE Comput. Soc. Conf. on Computer Vision and Pattern Recognition, Jun. 2009, pp. 104-111.

[4] Levin A et al., "Understanding and evaluating blind deconvolution algorithms," in Proc. IEEE Comput. Soc. Conf. on Computer Vision and Pattern Recognition, Jun. 2009, pp. 1964-1971.

[5] Levin A et al., "Efficient marginal likelihood optimization in blind deconvolution," in Proc. IEEE Comput. Soc. Conf. on Computer Vision and Pattern Recognition, Jun. 2011, pp. 2657-2664.

[6] Krishnan D, Tay T, and Fergus R, "Blind deconvolution using a normalized sparsity measure," in Proc. IEEE Comput. Soc. Conf. on Computer Vision and Pattern Recognition, Jun. 2011, pp. 233-240.

[7] Sun L B et al., "Edge-based blur kernel estimation using patch priors," in Proc. of IEEE Int. Conf. on Computational Photography, Apr. 2013, pp. 1-8, 19-21.

[8] Mai L and Liu F, "Kernel fusion for better image deblurring," in Proc. IEEE Comput. Soc. Conf. on Computer Vision and Pattern Recognition, Jun. 2015, pp. 371-380.

[9] Joshi N, Szeliski R and Kriegman D J, "PSF estimation using sharp edge prediction," in Proc. IEEE Comput. Soc. Conf. on Computer Vision and Pattern Recognition, Jun. 2008, pp. 3823-3830.

[10] Cho S and Lee S, "Fast motion deblurring," ACM Trans. on Graphs. vol. 28, no. 5, Article No. 145, 2009.

[11] Xu L and Jia J Y, "Two-phase kernel estimation for robust motion deblurring," in Proc. of European Conf. on Computer Vision, Sep. 2010, pp. 157-170.

[12] Pan J S et al., "Kernel estimation from salient structure for robust motion deblurring," Signal Process. Image Comm., vol. 28, no. 9, pp. 1156-1170, 2013.

[13] Zhong L et al., "Handling noise in single image deblurring using directional filters," in Proc. IEEE Comput. Soc. Conf. on Computer Vision and Pattern Recognition, Jun. 2013, pp. 612-619.

[14] Zhou Y P and Komodakis N, "A MAP-estimation framework for blind deblurring using high-level edge priors," in Proc. of European Conf. on Computer Vision, Sep. 2014, pp. 142-157.

[15] Li W, Zhang J and Dai Q H, "Robust blind motion deblurring using near-infrared flash image," J. Vis. Commun. and Image R. vol. 24, no.8, pp. 1394-1413, 2013.

[16] Li H S et al., "Joint motion deblurring with blurred/noisy image pair," in Proc. of Int. Conf. on Pattern Recognition, Jun. 2014, pp. 1020-1024.

[17] Shan Q, Xiong W, and Jia J, "Rotational motion deblurring of a rigid object from a single image," in Proc. IEEE Comput. Soc. Conf. on Computer Vision, Oct. 2007, pp. 1-8.

[18] Whyte O et al., " Non-uniform deblurring for shaken images," in Proc. IEEE Comput. Soc. Conf. on Computer Vision and Pattern Recognition, Jun. 2008, pp. 491-498.

[19] Tai Y, Tan P, and Brown M S, "Richardson-lucy deblurring for scenes under projective motion path," IEEE Trans. on Pattern Analysis and Machine Intelligence, vol. 33, no. 8, pp. 1603-1618, 2011.

[20] Nocedal J and Wright S, "Numerical Optimization," Springer Series in Operatins Research. Springer, 2006.

[21] Dong W S, Shi G M, and Li X, "Nonlocal image restoration with bilateral variance estimation: A low-rank approach," IEEE Trans. on Image Processing, vol. 22, no. 2, pp. 700–711, 2013.

[22] Xu L, Zheng S and Jia J Y, "Unnatural L0 sparse representation for natural image deblurring," in Proc. IEEE Comput. Soc. Conf. on Computer Vision and Pattern Recognition, Jun. 2013, pp. 1107-1114,.

[23] Wang Z *et al*., "Image quality assessment: from error visibility to structural similarity," IEEE Trans. on Image Processing, vol. 13, no. 4, pp. 600-612 , 2004.

[24] Tai Y and Lin S, "Motion-aware noise filtering for deblurring of noisy and blurry images," in Proc. IEEE Comput. Soc. Conf. on Computer Vision and Pattern Recognition, Oct 2012, pp. 17-24.